Mechanism of Dual Ferroic Properties Formation in Substituted M-Type Hexaferrites

A. V. Trukhanov, S. V. Trukhanov, L. V. Panina, V. G. Kostishin, V. A. Turchenko

Abstract—It has been shown that $BaFe_{12}O_{19}$ is a perspective room-temperature multiferroic material. A large spontaneous polarization was observed for the $BaFe_{12}O_{19}$ ceramics revealing a clear ferroelectric hysteresis loop. The maximum polarization was estimated to be approximately 11.8 $\mu C/cm^2$. The FeO_6 octahedron in its perovskite-like hexagonal unit cell and the shift of Fe^{3+} off the center of octahedron are suggested to be the origin of the polarization in $BaFe_{12}O_{19}$. The magnetic field induced electric polarization has been also observed in the doped $BaFe_{12-x-\delta}Sc_xM_\delta O_{19}$ ($\delta=0.05$) at 10 K and in the $BaSc_xFe_{12-x}O_{19}$ and $SrSc_xFe_{12-x}O_{19}$ (x = 1.3–1.7) M-type hexaferrites. The investigated $BaFe_{12-x}D_xO_{19}$ (x=0.1, D-Al^{3+}, In^{3+}) samples have been obtained by two-step "topotactic" reactions. The powder neutron investigations of the samples were performed by neutron time of flight method at High Resolution Fourier Diffractometer.

Keywords—Substituted hexaferrites, ferrimagnetics, ferroelectrics, neutron powder diffraction, crystal and magnetic structures.

I. INTRODUCTION

DURING the past time barium hexaferrites M-type-$BaFe_{12}O_{19}$ has been realized as an effective material for permanent magnets with high magnetic energy [1]; and as magnetic recording media of high density (with perpendicular type of magnetization) [1]; and as effective material for microwave and millimeter-wave device application (such as isolators, phase shitters and circulators) [2], [3].

The unit cell of $BaFe_{12}O_{19}$ has hexagonal symmetry [4] with the magnetic easy axis along the crystallographic c-axis. The crystal structure can be built up from the spinel block(s) interposed by hexagonal R block that contains the barium ions. Iron ions reside at five inequivalent crystallographic sites [5]. Three out of five are octahedral sites ($Fe1-2a$; $Fe4-4f_{VI}$ and $F5-12k$) while the other two are tetrahedral ($Fe3-4f_{IV}$) and five-fold bipyramidal sites ($Fe2-2b$). Below the Curie temperature 12 cations Fe^{3+} at 5 sublattices are ordered antiparallel. The total magnetization of M-type hexaferrites

results from the net momentsbetween the 12 magnetic ions on the five sublattices: 1*Fe1; 2*Fe2; 1*Fe3;2*Fe4 ;6*Fe5. At 0 K, $BaFe_{12}O_{19}$ was predicted from the model with eight spins up and four spins down resulting in 20μ_B per formula unit [6]. In recent years, there has been increasing interest in multiferroic materials. They provide a wide range of potential applications, such as multiple-state memory elements, novel memory media, transducers, and new functional sensors [7], [8]. However, materials with ferroelectricity and ferromagnetism coexistence are rare [9], [10] and mostly provide rather weak ferromagnetism. Because the multiferroism at room temperature is an essential issue for the realization of multiferroic devices that exploit the coupling between ferroelectric and ferromagnetic orders at ambient conditions. There are a lot of recently developed compounds $BaFeO_3$; $LiFe_2O_4$; $Pb_2Fe_2O_5$ [11]-[15]. Ba-hexaferrites considered as promising candidates for device application. Preparation of materials in which large ferroelectricity and strong ferromagnetism coexistence must be a milestone for modern electrics and functionalized materials [16]. Since large ferroelectric polarization was found in $PbFe_{12}O_{19}$ [15] and $BaFe_{12}O_{19}$ hexagonal M-type ferrites, it opened a new direction [17], [18]. There are two main mechanisms for electrical polarization in M-type hexaferrites: exchange-striction mechanism [19]-[21] and spin-current mechanism [22]. Exchange-striction mechanism was originally introduced to explain magnetoelectrical effect in Cr_2O_3, $RMnO_3$ (R=Ho and Tm), and $BaFe_{12}O_{19}$ [17]. Ferroelectricity is attributed to as symmetric-type interaction, i.e. crystallographic deformation induced by changing bonding as a result of a magnetic order. Sometimes, the combination between spin arrangement and crystallographic symmetry makes the local polarization align uniformly, and then ferroelectricity arises. This mechanism is with collinear spin configuration. Spin-current mechanism or inverse Dzyaloshinskii-Moriya mechanism is ascribed to noncollinear spiral magnetic structures with a cycloidal component. This mechanism is induced between noncollinear coupled spins at an angle and it leads to electric polarization. This can be regarded as an inverse effect of the antisymmetric DM interaction in which two noncollinear coupled magnetic moments displace the ligand intervening between them through the electron-lattice interaction. When the magnetic moments are aligned in a cycloidal spiral manner, the direction of the local electric polarization induced by the inverse DM interaction is uniform in the system, and the total electric polarization can be finite in the direction perpendicular to both the spin spiral axis and the magnetic modulation vector **Q**. Phenomenological treatments

A. V. Trukhanov is now with National University of Science and Technology MISiS, 119049, Leninsky Prospekt 4, Moscow, Russia (phone: +375-29-518-63-06, e-mail: truhanov86@mail.ru) and was withSSPA "Scientific and practical materials research centre of NAS of Belarus", 220072, P. Brovki str. 19, Minsk, Republic of Belarus.

S. V. Trukhanov is now with SSPA "Scientific and practical materials research centre of NAS of Belarus", 220072, P. Brovki str. 19, Minsk, Republic of Belarus (e-mail: truhanov@physics.by).

V. G. Kostishinis and L. V. Paninais are now with National University of Science and Technology MISiS, 119049, LeninskyProspekt 4, Moscow, Russia (e-mail: drvgk@mail.ru, drpanina@mail.ru).

V. A. Turchenkois now with Joint Institute for Nuclear Research, 141980, Joliot-Curie str. 6, Dubna, Russia (e-mail: turchenko@mail.ru).

World Academy of Science, Engineering and Technology
International Journal of Materials and Metallurgical Engineering
Vol:10, No:8, 2016

using Landau theory have also been reported. These theoretical studies explain well the magnetically induced ferroelectricity in $TbMnO_3$ and many other magnetically induced ferroelectrics showing spiral magnetic orders with cycloidal components, e.g., cycloidal and transverse-conical orders [23].

II. EXPERIMENTAL

Polycrystalline samples $BaFe_{11.9}D_{0.1}O_{19}$ (D = Al^{3+} and In^{3+}) were prepared by the conventional ceramic method using, in appropriate proportions, oxides Fe_2O_3, Al_2O_3/In_2O_3, and carbonate $BaCO_3$. The starting compositions were subjected to synthesis at 1200 °C (6 h) and were annealed at 1300 °C (6 h) in air. Then, the annealing samples were slowly cooled down (100 °C/h). The formation of $BaFe_{12-x}D_xO_{19}$ (D = Al^{3+} and In^{3+}; x = 0.1) powder can be represented as:

$$BaCO_3 + (5.95)Fe_2O_3 + (0.05)D_2O_3 \rightarrow BaFe_{11.9}D_{0.1}O_{19} + CO_2 \uparrow$$
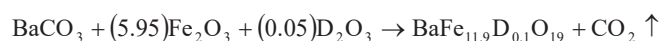
A preliminary structural and qualitative phase analysis of the samples was conducted at room temperature on a diffractometer DRON-3M in Cu-Kα radiation with 0.05° scanning step. The investigation of the crystalline and magnetic structures of $BaFe_{11.9}D_{0.1}O_{19}$ (D = Al^{3+} and In^{3+}) samples was carried out in a wide temperature range (from 4 K to 730 K) with the High Resolution Fourier Diffractometer, or HRFD [24]. HRFD is a time-of-flight diffractometer on IBR-2 in Dubna with a relatively large (21.131 m) path-length from the moderator to the detector and has an exceptionally high resolution ($\Delta d/d0 \approx 0.001$), which is also virtually independent of the interplanar distances, d_{hkl}, over a wide range. High-resolution neutron diffraction was measured by two detectors located at average scattering angles ±152°. This allows receiving data in the range of interplanar distances from 0.6 to 3.6 °A. Calculations of the experimental neutron TOF data have been performed by the Rietveld full-profile analysis using the software MRIA and FullProf, with built-in tables for the lengths of coherent scattering and magnetic form factor. The resolution of HRFD was determined in a separate experiment by using the standard Al_2O_3. The microstructural parameters have been determined by broadening the individual diffraction peaks. The Curie temperature was determined by the ponderomotive method in the dimension of the specific magnetization in the external magnetic field 0.86 T. Field dependences of magnetization for both compositions were measured at 300 K by using a vibrating sample magnetometer, the Liquid Helium Free High Field Measurement System from Cryogenic Ltd.

III. RESULTS AND DISCUSSION

A. Crystal Structure

Polycrystalline samples $BaFe_{11.9}D_{0.1}O_{19}$(D = Al and In) are single-phase and can be described by the space group P63/mmc (no 194). Precise determination of the lattice parameters and clarification of the atomic structure of the

samples were carried out by neutron diffraction in a wide temperature range from 4.2 to 730 K. A high-resolution diffractometer and correspondingly large number of well-separated peaks ensure good convergence of the minimization process. In the calculation, we took into account the thermal vibrations of atoms in the isotropic approximation and the magnetic hexaferrite structure in the collinear approximation. Low values of $\chi 2$ and others parameters (R_{wp}, R_{exp}, R_{Mag}) indicate good agreement among the theoretical and experimental models. The temperature dependences of the lattice parameters of the unit cells of the substituted barium hexaferrites are shown in Fig. 1. The small volume of the unit cell of $BaFe_{11.9}Al_{0.1}O_{19}$, unlike that of barium ferrite doped by indium, is explained by the larger value of ionic radius of In^{3+} (0.790°A) unlike that of the Al^{3+} (0.530°A) ion. Structural transformations were not observed in both compounds over the entire temperature range from 4.2 to 750 K. The partial replacement of iron by diamagnetic ions affects the thermal expansion coefficient (TEC) from the value of α =3.229*10^{-5} 1/K, when iron ions are partially substituted by aluminum ions up to α_V = 4.342*10^{-5} 1/K, when the barium ferrite is doped with indium ions. In addition, there is a dependence of linear TEC from crystal directions. For example, in Al-doped ferrite, linear TEC have the following values: along the hexagonal axis, α_c = 14.33*10^{-6} 1/K, whereas on the reference plane, α_a = 8.91*10^{-6} 1/K; for In-doped ferrites, α_a = 10.90*10^{-6}1/K, and α_c =19.37*10^{-6} 1/K, respectively.
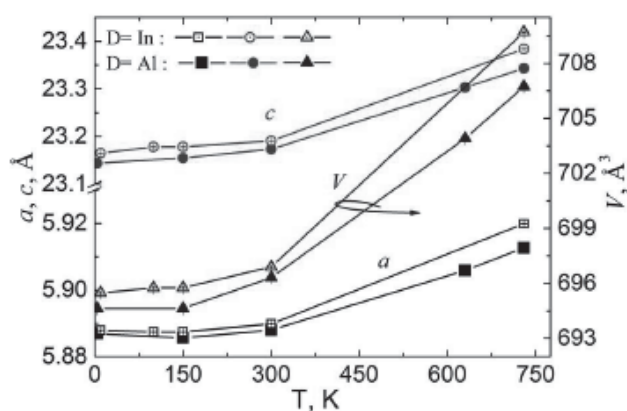

Fig. 1 Temperature dependence of lattice parameters (a and c, left scale) and volume of unit cell (V, right scale) of $BaFe_{11.9}D_{0.1}O_{19}$

B. Magnetic Properties

Fig. 2 shows temperature dependences of specific magnetization of $BaFe_{11.9}D_{0.1}O_{19}$(D = $Al^{3+}$and In^{3+}). In accordance with these dependences, the ferrimagnetic-paramagnetic phase transition occurs at Tc ≈ 705 K and 695 K, respectively. The temperatures of the phase transition are 20–30 K less than the Curie temperature of pure barium ferrite $BaFe_{12}O_{19}$ which confirms the substitution of iron by diamagnetic ions. The number of magnetic neighbors of iron ions decreases and the long-range magnetic order is interrupted as the ambient temperature of the samples increases. It should be noted that for In-doped ferrites, the

World Academy of Science, Engineering and Technology
International Journal of Materials and Metallurgical Engineering
Vol:10, No:8, 2016

phase transition temperature is about 10 K lower than that for Al-doped.
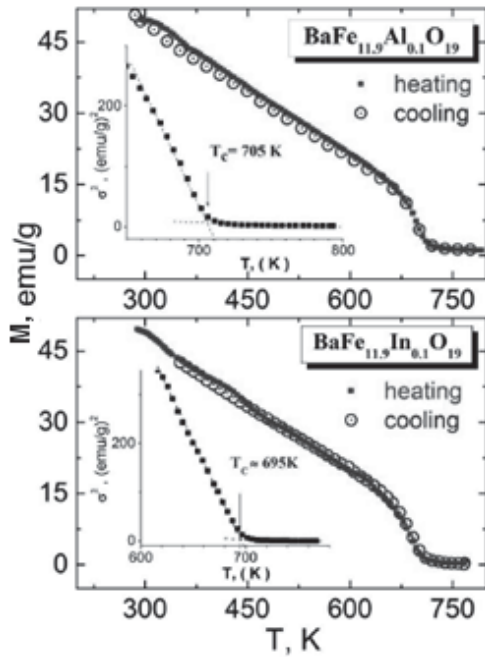
Fig. 2 Temperature dependences of the specific magnetization of $BaFe_{11.9}D_{0.1}O_{19}$ (D = Al and In). In the inset points of magnetic phase transition are shown

Fig. 3 shows field dependences of specific magnetization of $BaFe_{11.9}D_{0.1}O_{19}$(D = Al^{3+} and In^{3+}). The In-substituted sample shows a higher coercitivity ($H_c \sim 0.1$ T) in comparison with the sample doped with Al ions ($H_c \sim 0.007$ T). The difference of H_c values achieves more than a single order of magnitude. The magnetization curve of the $BaFe_{11.9}Al_{0.1}O_{19}$ sample reaches saturation at 0.3–0.5 T, whereas the magnetization for the In-doped sample does not achieve saturation even in the field of 2 T.
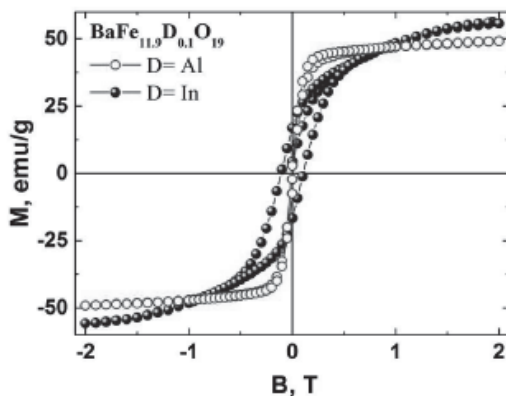

Fig. 3 Field dependences of specific magnetization of $BaFe_{11.9}D_{0.1}O_{19}$ (D = Al and In)

This difference in the behavior of magnetization can be explained by the frustrated magnetic structure of the $BaFe_{11.9}In_{0.1}O_{19}$ sample, as a result of the higher crystal structure distortion due to substitution of iron by In ions with larger ionic radius. This incommensurable substitution leads to an increase of Fe-O bond lengths and to distortion of anion sublattice.

C. Electric Properties

Ferroelectric properties were characterized by using polarization hysteresis and pulse polarization measurements. The electric field-induced polarization (P) demonstrated at Fig. 4. It is shows the ferroelectric hysteresis loops of $BaFe_{11.9}Al_{0.1}O_{19}$ (Fig. 4 (a)) and $BaFe_{11.9}In_{0.1}O_{19}$ (Fig. 4 (b)) at room temperature in the electrical field up 100 kV/m. During the ferroelectric measurement, the specimen was connected parallel to a capacitor of 0.5 µF for compensation.

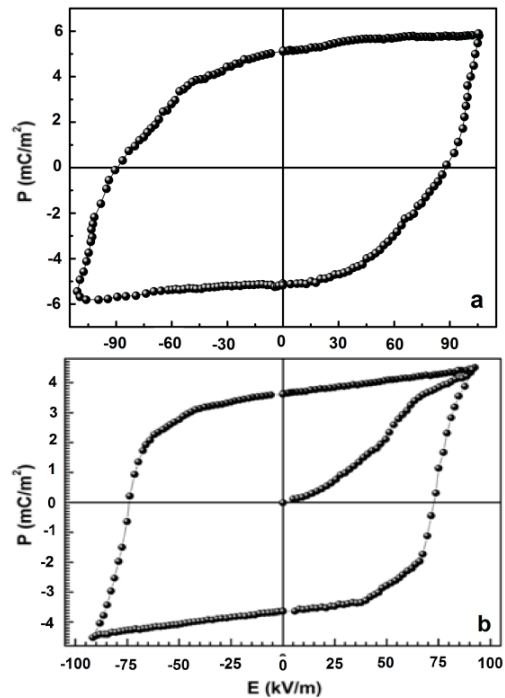Fig. 4 Ferroelectric hysteresis loops of $BaFe_{11.9}Al_{0.1}O_{19}$ (a) and $BaFe_{11.9}In_{0.1}O_{19}$ (b) at room temperature

Measurements were carried out by a triangular wave voltage. Evidence for the characterization of ferroelectric state of $BaFe_{11.9}D_{0.1}O_{19}$ ceramic is polarization cycle exhibiting clear ferroelectric hysteresis loops under applied electric field. The maximum polarization (P_{MAX}), remanent polarization (P_r) and the coercive electric field (E_C) obtained from the ferroelectric hysteresis loop in Fig. 4 for $BaFe_{11.9}Al_{0.1}O_{19}$ were approximately ~ 5.89 mC/m^2, ~ 5.13 mC/m^2 and ~ 86 kV/m respectively and for $BaFe_{11.9}In_{0.1}O_{19}$ were approximately ~ 4.7 mC/m^2, ~ 3.8 mC/m^2 and ~ 75 kV/m, respectively. The coexistence of electrical polarization and magnetization in single-phase samples is an evidence of the multiferroic properties, and demonstration of multiferroic properties at room temperatures is opportunity for practical application of such kind materials.

World Academy of Science, Engineering and Technology
International Journal of Materials and Metallurgical Engineering
Vol:10, No:8, 2016

D. Magnetic Structure

The dependences of the main Fe-O bond lengths for the $BaFe_{11.9}Al_{0.1}O_{19}$ and $BaFe_{11.9}In_{0.1}O_{19}$ samples refined from NPD versus temperature are shown in Figs. 5 and 6, respectively. For the studied sample, was not found any abrupt changes of the internal structural parameters over the entire temperature range from 4 K up to 750 K.
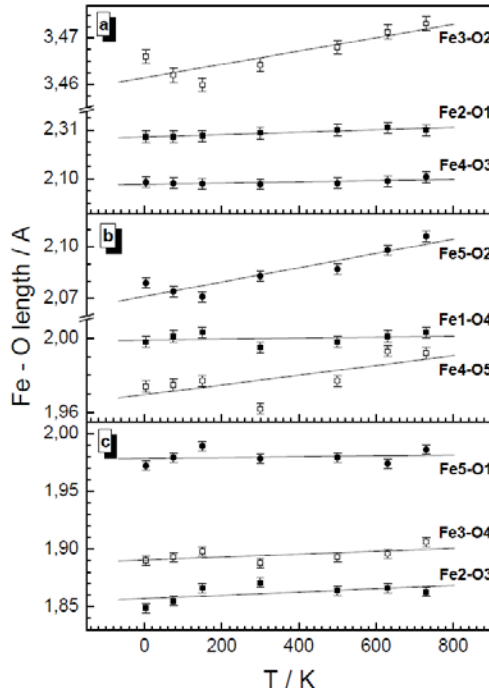

Fig. 5 The temperature dependence of the main Fe-O bond lengths for the $BaFe_{12-x}Al_xO_{19}$ (x=0.1) sample refined from NPD data

All the bond lengths for $BaFe_{11.9}Al_{0.1}O_{19}$ decrease with temperature decreasing (Fig. 5). The most changes in the bond lengths are detected for the Fe3 cation relative to the O2 cation, for the Fe4 cation relative to the O5 cation and for the Fe5 cation relative to the O2 anion.

For the studied $BaFe_{11.9}In_{0.1}O_{19}$ sample, was not found any abrupt changes of the internal structural parameters over the entire temperature range from 10 K up to 730 K. The majority of the bond lengths decreases with temperature decreasing. The Fe1-O4, Fe2-O3, and Fe3-O2 bond lengths increase with temperature decreasing (Fig. 6). The most changes in the bond lengths are detected for the Fe3 cation relative to the O2 cation, for the Fe2 cation relative to the O3 cation, and for the Fe1 cation relative to the O4 cation.

The dependences of the main Fe-O-Fe bond angles of $BaFe_{11.9}Al_{0.1}O_{19}$ and $BaFe_{11.9}In_{0.1}O_{19}$ samples refined from NPD versus temperature are shown in Figs. 7 and 8, respectively.
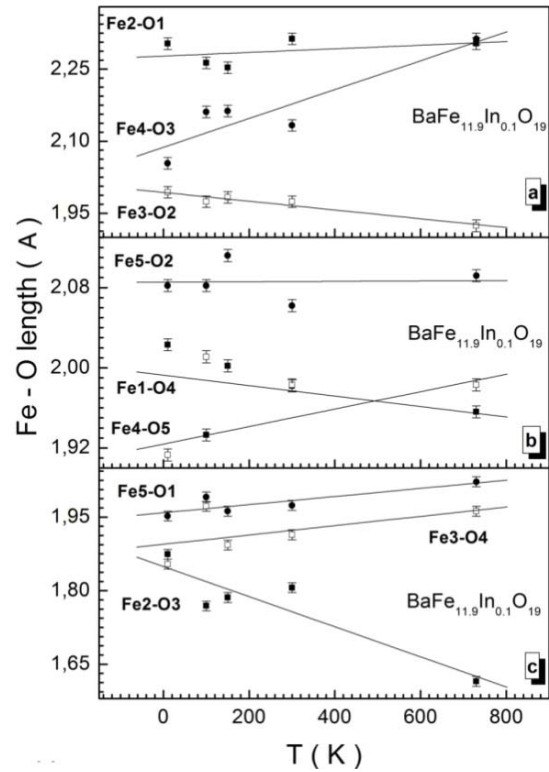

Fig. 6 The temperature dependence of the main Fe-O bond lengths for the $BaFe_{11.9}In_{0.1}O_{19}$ sample refined from NPD data
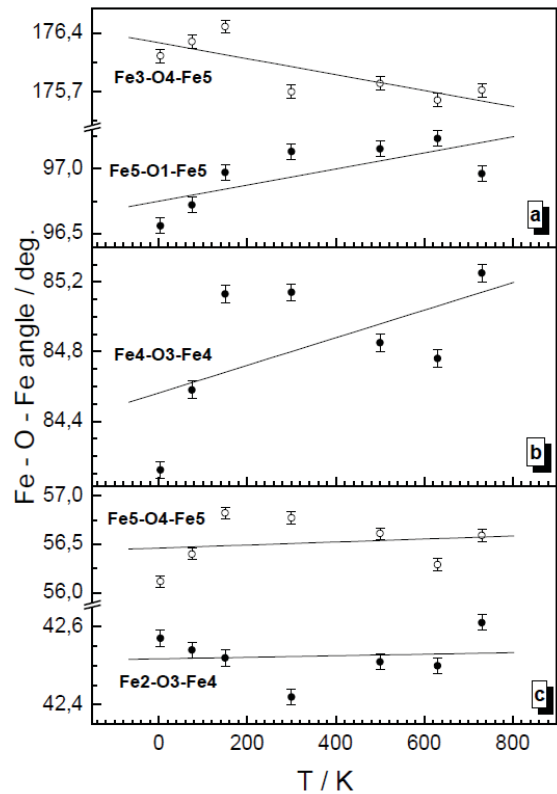

Fig. 7 The temperature dependence of the main Fe-O-Fe bond angles for the $BaFe_{12-x}Al_xO_{19}$ (x=0.1) sample refined from NPD data

World Academy of Science, Engineering and Technology
International Journal of Materials and Metallurgical Engineering
Vol:10, No:8, 2016

Almost all from the bond angles of $BaFe_{11.9}Al_{0.1}O_{19}$ decrease with temperature decreasing except for the Fe3-O4-Fe5 (Fig. 7). The most changes in the $BaFe_{11.9}Al_{0.1}O_{19}$ bond angles are detected for the Fe4-O3-Fe4, Fe5-O1-Fe5 (they decrease) and Fe3-O4-Fe5 (it increases) as temperature decreases. Almost all from the bond angles of $BaFe_{11.9}In_{0.1}O_{19}$ decrease with temperature decreasing except for the Fe3-O4-Fe5; Fe4-O3-Fe4 and Fe5-O2-Fe5 (Fig. 8). The most changes for $BaFe_{11.9}In_{0.1}O_{19}$ in the bond angles are detected for Fe4-O3-Fe4 and Fe5-O2-Fe5. So, we can conclude that the nature of substitution ion leads to different distortion in the crystal structure and in can be the reason of different electric and magnetic properties. We focus on the behavior of the internal structural parameters as a function of temperature since it may help to understand the magnetic and dielectric properties.
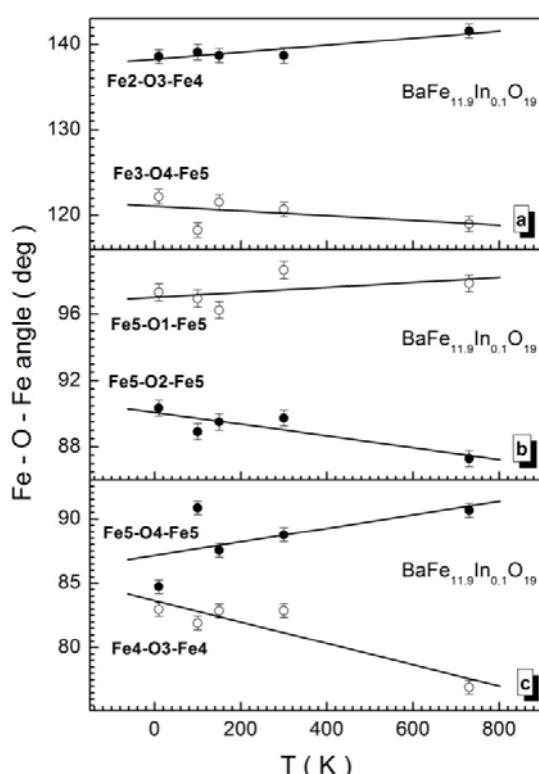

Fig. 8 The temperature dependence of the main Fe-O-Fe bond angles for the $BaFe_{11.9}In_{0.1}O_{19}$ sample refined from NPD data

E. Mechanism of Dual Ferroic Properties Formation

Careful analysis of the unit model structure suggests a perovskite-like crystal structure with one distorted FeO_6 oxygen octahedron in hexagonal $BaFe_{12-x}D_xO_{19}$ (where D is diamagnetic ion). Each hexagonal $BaFe_{12-x}D_xO_{19}$ model has one FeO_6 oxygen octahedron in a sub-unit cell. In a normal octahedron, Fe cation is located at the center of an octahedron of oxygen anions (Fig. 9 (a)). However, in the unit cell of $BaFe_{12-x}D_xO_{19}$ below the Curie temperature, there is also a distortion to a lower-symmetry phase accompanied by the shift off-center of the small Fe cation (Fig. 9 (b)). Fe cation shifts away from the center along b-axis, while O5 and O6 shift off their original positions of the octahedron along the opposite directions of *a* axis, which leads to the distortion of

O5–Fe–O6 bond away from straight line. The spontaneous polarization occurs due to the two shifts in 12k oxygen octahedron. So, neutron powder diffraction data (bond length and angels, collinear direction of magnetization vector) indicate not only in which exactly position this iron cation is located – 12k position and even preferable mechanism of multiferroic property formation (exchange-striction mechanism).
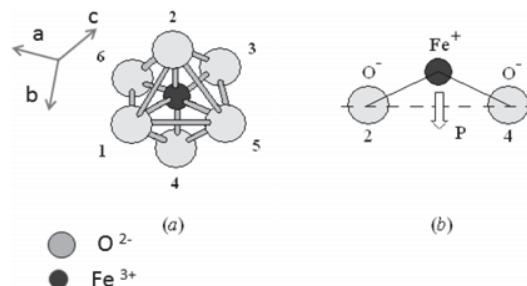

Fig. 9 Illustration of the occurrence of the polarization due to a distorted oxygen octahedron in $BaFe_{12-x}D_xO_{19}$ (x=0.1). In (a) - a normal octahedron with small Fe–cation in the center position (Fe–cation and oxygen anions in positions 2 and 4 are in the plane (110, 001)); in (b) – a distorted O-Fe-O bond with an open angle

IV. CONCLUSION

By high resolution neutron diffraction and vibration magnetometry the crystal and magnetic structure and magnetic properties of the $BaFe_{11.9}D_{0.1}O_{19}$ (D=Al^{3+}, In^{3+}) samples were investigated over a wide temperature range of 4-730 K. The lattice parameters and atomic coordinates were Rietveld refined with space group ($P6_3/mmc$) by Fullprof program. The coefficients of linear and volume thermal expansion were calculated. The temperature dependences of the main Fe-O bond lengths and Fe-O-Fe bond angles were constructed. The temperature and field dependences of specific magnetization were investigated. It is established that the ferrimagnet-paramagnet phase transition is a standard second-order one. From the macroscopic magnetization measurement, the Curie temperature and ordered magnetic moment per nominal iron ion are obtained. It is shown that the magnetic structure of the investigated samples over the entire temperature range in good agreement with Gorter's model according to which the magnetic moments of the Fe^{3+} cations are oriented along the hexagonal axis which is the axis of easy magnetization. The observed decrease of the specific magnetization with temperature increasing due to the destroy of the intersublattice exchange interactions initially and of the intrasublattice Fe^{3+}-$O^{2-}Fe^{3+}$ indirect superexchange interactions further. The main contribution to the weakening of the magnetic ordering at low temperatures follows from the destruction of the intersublattice exchange interactions between Fe3, Fe4, Fe5 sublattices. Fe4 and Fe5 cations may be responsible for the polarization origin. It is concluded that the magnetic phase transition that occurs for the $BaFe_{11.9}Al_{0.1}O_{19}$ at ~705 K and for $BaFe_{11.9}In_{0.1}O_{19}$ at ~695 K is a second-order thermodynamic phase transition from the ferrimagnetic to paramagnetic state. The magnetic structure model is proposed.

World Academy of Science, Engineering and Technology
International Journal of Materials and Metallurgical Engineering
Vol:10, No:8, 2016

Simultaneous occurrence of ferroelectricity and strong ferromagnetism at room temperature have been observed in $BaFe_{11.9}D_{0.1}O_{19}$ ($D=Al^{3+}$, In^{3+}). The maximum polarization (P_{MAX}), remanent polarization (P_r) and the coercive electric field (E_C) obtained from the ferroelectric hysteresis loop for $BaFe_{11.9}Al_{0.1}O_{19}$ were approximately ~5.89 mC/m², ~5.13 mC/m² and ~86 kV/m, respectively, and for $BaFe_{11.9}In_{0.1}O_{19}$ were approximately ~4.7 mC/m², ~3.8 mC/m², and ~75 kV/m, respectively. The most likely reasons and the mechanism of multiferroic property formation (exchange-striction mechanism) are discussed.

ACKNOWLEDGMENT

REFERENCES

[1] E. Richter, T. J. E. Miller, T. W. Neumann and T. L. Hudson The ferrite permanent magnet ac motor-a technical and economical assessment, *IEEE Trans. Industry Applications*, 1985, Vol. 1A-21, No. 4, pp. 644-650.

[2] P Shi, H How, X Zuo, SD Yoon, SA Oliver, C Vittoria MMIC circulators using hexaferrites, *IEEE Transactions on magnetic,* 2001,37 (4), pp. 2389-2391.

[3] V.G. Harris, Zh. Chen, Y. Chen, et al., Ba-hexaferrite films for next generation microwave devices *J. Appl. Phys.*, 2006, 99, 08M911.

[4] R.C. PullarHexagonal ferrites: a review of the synthesis, properties and applications of hexaferrite ceramics*Prog. Mat. Sci.*, 2012, 57, pp. 1191-1334.

[5] E.W. Gorter Crystal structure of M-type hexaferrites*Proc. IEEE Suppl.*,1957, 104 B, pp. 225-237.

[6] J. Smit, H.P.J. Wijn Ferrites, *Hume Press Ltd.*1959, P. 142.

[7] D.I. Khomskii, Multiferroics: Different ways to combine magnetism and ferroelectricity*Journal of Magnetism and Magnetic Materials*2006, 306, pp.1-8.

[8] M. Fiebig, ThLottermoser, D. Frohlich, A.V. Goltsev, R.V. Pisarev, Observation of coupled magnetic and electric domains*Nature*, 2002, 419, pp.818-820.

[9] N.A. Hill, Why Are There so Few Magnetic Ferroelectrics? *The Journal of Physical Chemistry B*2000, 104, pp.6694-6709.

[10] N. Hur, S. Park, P.A. Sharma, J.S. Ahn, S. Guha, S.W. Cheong, Electric polarization reversal and memory in a multiferroic material induced by magnetic fields *Nature*2004, 429, pp. 392-395.

[11] N. Ikeda, H. Ohsumi, K. Ohwada, K. Ishii, T. Inami, K. Kakurai, Y. Murakami, K. Yoshii, S. Mori, Y. Horibe, H. Kito, Ferroelectricity from iron valence ordering in the charge-frustrated system LuFe2O4 *Nature*2005, 436, pp. 1136-1144.

[12] H. J. Xiang, M. H. Whangbo, Charge Order and the Origin of Giant Magnetocapacitance in LuFe2O4 *Physical Review Letters*2007, 98, pp. 246403.

[13] S. Ryu, J.Y. Kim, Y.H. Shin, B.G. Park, J.Y. Son, H.M. Jang,Enhanced magnetization and modulated orbital hybridization in epitaxially constrained BiFeO3 thin films with rhombohedral symmetry *Chemistry of Materials*, 2009, 21, pp.50505057.

[14] M. Wang, G.L. Tan, Multiferroic properties of Pb2Fe2O5 ceramics *Materials Research Bulletin*2011, 46, pp. 438-445.

[15] G. L. Tan, M. Wang, Multiferroic Properties of BaFe12O19 *Ceramics Journal of Electroceramics*2011, 26, pp.170-178.

[16] J. Hemberger, P. Lunkenheimer, R. Fichtl, H.A. Krug von nidda, V. Tsurkan, A. Loidl, Relaxor ferroelectricity and colossal magnetocapacitive coupling in ferromagnetic CdCr2S4 *Nature* 2005, 434, pp.364-371.

[17] V.G. Kostishyn, L.V. Panina, A.V. Timofeev et al., Dual ferroic properties of hexagonal ferrite ceramics BaFe12O19 and SrFe12O19 *Journal of Magnetism and Magnetic Materials*. 2016, 400, pp. 327-332

[18] A.V. Trukhanov, V.A. Turchenko, I.A. Bobrikov et al Crystal structure and magnetic properties of the BaFe12−xAlxO19 (x=0.1–1.2) solid solutions *Journal of Magnetism and Magnetic Materials*. 2015, 393, pp.253-259.

[19] Sergienko IA, Sen C, Dagotto E. Ferroelectricity in the Magnetic E-Phase of Orthorhombic Perovskites *Physical Review Letters*2006, 97:227204.

[20] Pomjakushin VY, Kenzelmann M, Do¨ nni A, Harris AB, Nakajima T, et al. Evidence for large electric polarization from collinear magnetism in TmMnO3*New Journal of Physics*2009, V.11:043019.

[21] Picozzi S, Yamauchi K, Sanyal B, Sergienko IA, Dagotto E. Dual Nature of Improper Ferroelectricity in a MagnetoelectricMultiferroic *Physical Review Letters* 2007, 99:227201.

[22] Katsura H, Nagaosa N, Balatsky AV. Spin current and magnetoelectric effect in noncollinear magnets *Physical Review Letters*2005. 95:057205

[23] Tsuyoshi Kimura Magnetoelectric Hexaferrites*Annu. Rev. Condens.Matter Phys.* 2012. 3:93–110.

[24] A. M. Balagurov, Scientific Reviews: High-Resolution Fourier Diffraction at the IBR-2 Reactor *Neutron News*, 2005, 163, pp. 8-12.